

# Numerical Study on Indoor Wideband Channel Characteristics with Different Internal Wall

Xue-Song YANG, Zhi-Ming TIAN, Jia-Jie YUAN, Yi-Teng ZHANG, Wei SHAO

School of Physical Electronics, University of Electronic Science and Technology of China,  
North Jianshe Road, Section 2, No. 4, Chengdu, 610054, China

xsyang@uestc.edu.cn

**Abstract.** Effects of material and configuration of the internal wall on the performance of wideband channel are investigated by using the Finite Difference Time-Domain (FDTD) method. The indoor wideband channel characteristics, such as the path-loss, Root-Mean-Square (RMS) delay spread and number of the multipath components (MPCs), are presented. The simulated results demonstrate that the path-loss and MPCs are affected by the permittivity, dielectric loss tangent and thickness of the internal wall, while the RMS delay spread is almost not relevant with the dielectric permittivity. Furthermore, the comparison of simulated result with the measured one in a simple scenario has validated the simulation study.

## Keywords

Finite Difference Time-Domain (FDTD), indoor wideband channel, internal wall, simulation.

## 1. Introduction

For an efficient setup of indoor wideband wireless network, the characterization of the radio propagation channel is necessary. In indoor wideband wireless communications, the signal arriving at the receiver consists of multipath components (MPCs), which are resulted from the interaction of the transmitted signal with the surrounding scatterers, including the surrounding wall. Many research results have been reported about the indoor wideband channel models [1-7], which are mostly based on some special indoor environments. It is obvious that the indoor channel model is closely related to the indoor environment, including the building structures and materials.

The building structures and materials are different from country to country. Among all the factors, the material of internal wall is a very important one to affect the channel performance. The internal wall is mostly made of brick or reinforced concrete in China and some other countries [4-6]. In [7], the effects of building structures on the line of sight (LOS) channel characteristics are investigated by using ray-tracing method, where the dielectric parameters of the exterior walls, internal walls, ceilings/floors,

windows and doors were adjusted synchronously, consequently, the relation between the specific building factor and the channel model parameters is not so clear. In the office environment, since the internal wall is a key difference in different countries, it is valuable to investigate the effect of the internal wall on the channel characteristics.

The Finite Difference Time Domain (FDTD) method, which is a full-wave analysis approach and has obvious advantages in emulating the electromagnetic waves transmission in small space, has been successfully used to predict the performance of radio channel [8-11]. In this paper, the effects of the permittivity, dielectric loss tangent and thickness of the internal wall on the non-line of sight (NLOS) channel performance are studied by the FDTD method.

## 2. Channel Characteristics

Many parameters can be used to depict the channel performance. In this paper, the path loss, Root-Mean-Square (RMS) delay spread and number of MPCs of the indoor wideband channel, are investigated.

The received power can be calculated based on the received signal

$$P = \int_{-\infty}^{+\infty} f^2(t) dt \quad (1)$$

where  $f(t)$  is the electric field of the received signal.

The channel impulse response is the most important channel characteristic. Since the received signal in an indoor wideband system consists of MPCs, the complex channel impulse response can be written as

$$h(t) = \sum_{k=1}^N a_k \delta(t - \tau_k) \quad (2)$$

where  $a_k$  and  $\tau_k$  are the amplitude and time delay of the  $k$ th MPC, respectively, and  $N$  is the total number of MPCs.

The path loss, which can be used to predict the power level of the system at a distance and the coverage range of the base station, is another important characteristic. The path loss at an observation point can be obtained by sub-

tracting the received power from the transmission power of the transmitting (Tx) antenna. In this work, the signal performance in an indoor space with an internal wall is simulated by FDTD. Since the internal wall causes an excess power loss, the path loss should include the effect of the obstruction of the internal wall, and is expressed as

$$PL(d) = PL(d_0) + PL_{obs} + 10\gamma \log\left(\frac{d}{d_0}\right) \quad (3)$$

where  $PL(d_0)$  is the path loss at a reference distance  $d_0$  (usually  $d_0 = 1$  m),  $PL_{obs}$  is the path loss arisen from the internal wall, and  $\gamma$  is the path loss decay exponent.

The RMS delay spread ( $\tau_{RMS}$ ) is used to quantify the time dispersion of the wideband multipath channel. It gives an indication of potential inter-symbol interference (ISI). It is defined as the square root of the second central moment of power delay profile and expressed as

$$\tau_{rms} = \sqrt{\frac{\sum_k a_k^2 \tau_k^2}{\sum_k a_k^2} - \left(\frac{\sum_k a_k^2 \tau_k}{\sum_k a_k^2}\right)^2} \quad (4)$$

Besides, the number of MPCs, which can be used to assess the extent of scattering in an indoor environment, is also a significant characteristic in the indoor wideband channel modeling.

### 3. Simulation Setup

The simulated indoor environment is a typical office, as shown in Fig. 1. It is a room with dimensions of  $6.36 \text{ m} \times 6.42 \text{ m} \times 3.90 \text{ m}$ . This room includes exterior walls, an internal wall, a floor, a ceiling, windows and doors. The internal wall splits the room into two compartments, with a door at the edge of the internal wall.

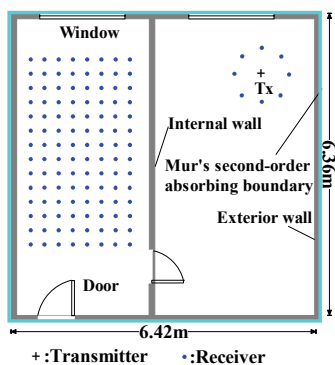


Fig. 1. Geometry of the indoor environment.

The whole simulation progress is performed with in-house software, of which the core is FDTD. The boundary of the simulation space, which is located at the outside surface of the exterior walls, is the Mur's second-order absorbing boundary condition. The Tx signal is the first-order Gaussian pulse, with center frequency of 600 MHz

and bandwidth of 350 MHz, i.e., from 425 MHz to 775 MHz. The whole simulation space is divided into discrete grid cells, with the grid size of 0.03 m (about  $\lambda/13$  at 775 MHz) [9].

The Tx antenna is an ideal dipole, located in the right side compartment at a fixed position, with a height of 1.5 m. Without any receiving (Rx) antenna, some electric field observation points are used to monitor the received signal. The 112 observation points, which are arranged in an  $8 \times 14$  rectangle grid, with the interspacing of 30 cm, are located in the left-hand side compartment, at the same height as the Tx antenna.

In the simulation, the permittivity  $\epsilon_r$ , dielectric loss tangent  $\tan(\delta)$  and thickness  $H$  of the internal wall are changed respectively, with the other building parameters fixed, as listed in Tab. 1. The received signals at all observation points can be obtained by FDTD simulation. Simulation of 112 observation points costs about 14 minutes of CPU time and 1.35 GB of memory, on a computer with Inter(R) Xeon(R) E5520 2.27 GHz CPU. With the received signal, the Channel Impulse Response (CIR), including the amplitude  $a_k$  and time delay  $\tau_k$ , are extracted with the CLEAN algorithm [12]. Afterwards, the path-loss and RMS delay spread are calculated by (2) and (3).

## 4. Simulation Results and Data Analysis

### 4.1 Path Loss at Reference Point

Firstly, the path loss at a reference point (usually with a Tx-Rx distance of  $d_0 = 1$  m) in free space is calculated. Eight observation points in the right-hand side compartment are equally distributed at a circle with radius of 1 m, centered at the Tx antenna, as shown in Fig. 1. By averaging the received power at the eight receiving points, the mean path loss  $PL(d_0)$  at the reference point with Tx-Rx distance of  $d_0 = 1$  m is obtained, which is 35.96 dB.

### 4.2 Different Permittivity of Internal Wall

In this study, the dielectric loss tangent  $\tan(\delta)$  and the thickness  $H$  of the internal wall are set to be 0.02 and 12 cm respectively, and the permittivity of the internal wall  $\epsilon_r$  is variable.

The path-loss, Cumulative Distribution Function (CDF) of RMS delay spread and number of MPCs of 112 observation points for each permittivity are calculated and shown in Fig. 2, respectively. As shown in Fig. 2(a), and the following Figs. 4(a) and 6(a), the data are fitting to straight lines by equation (3). Besides, based on the RMS delay spread and number of MPCs of all 112 received signals, the mean  $\tau_{RMS}$  and mean number of MPCs are calculated. The  $PL_{obs}$ ,  $\gamma$ , mean  $\tau_{RMS}$  and mean number of MPCs versus  $\epsilon_r$  are plotted in Fig. 3.

	$\epsilon_r$	$\tan(\delta)$	$H(\text{cm})$
exterior walls & ceiling & floor	8	0.04	12
doors	3	0.001	6
windows	2.2	0.007	6

Tab. 1. Parameters for other building structures.

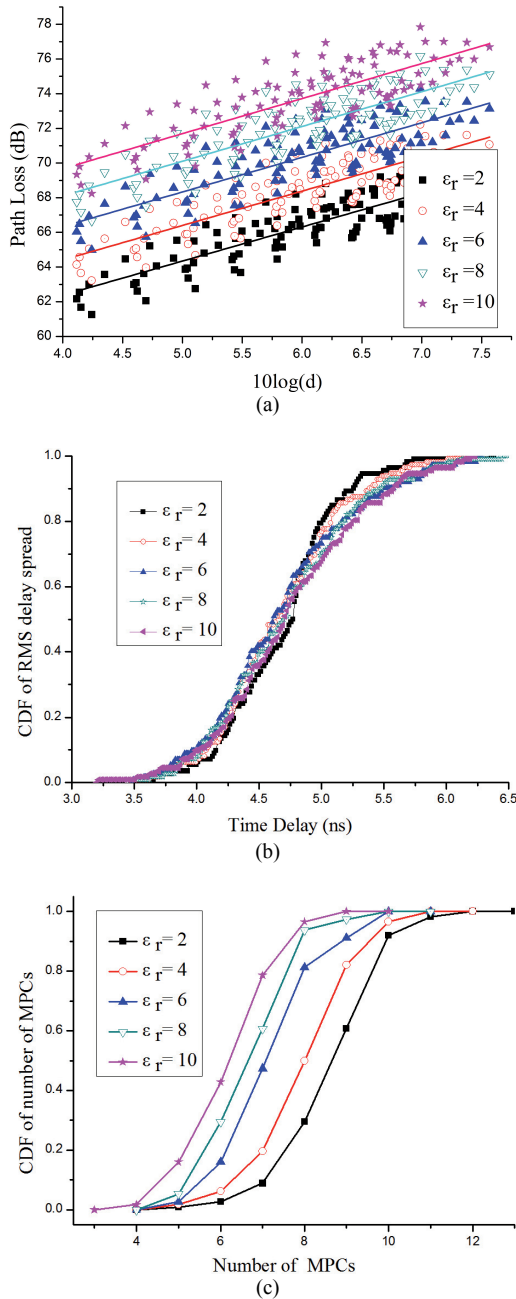


Fig. 2. Path-loss model, CDF of RMS delay spread and CDF of number of MPCs for different permittivity. (a) Path-loss model for different permittivity. (b) CDF of RMS delay spread for different permittivity. (c) CDF of number of MPCs for different permittivity.

From Figs. 2(a) and 3(a), it can be seen that with the increasing of internal wall permittivity  $\epsilon_r$ , the  $PL_{obs}$  increases linearly and  $\gamma$  increases slightly. From Figs. 2(b)

and 3(b), it can be found that the mean  $\tau_{RMS}$  is almost nothing to do with the  $\epsilon_r$ , which means that changing the  $\epsilon_r$  has no effect on the interference between multipath signals. From Figs. 2(c) and 3(b), it can be seen that the number of MPCs decreases as the  $\epsilon_r$  increases.

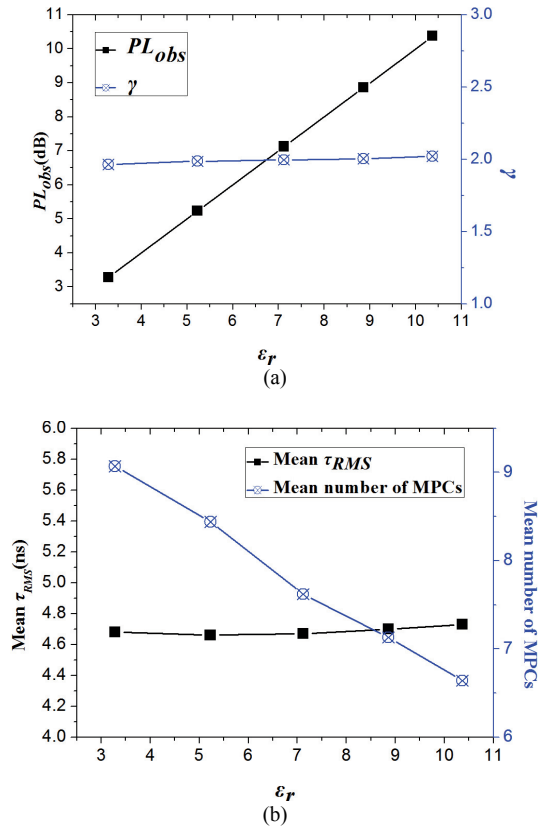


Fig. 3. Relation of path loss  $PL_{obs}$ ,  $\gamma$ , mean  $\tau_{RMS}$  and mean number of MPCs, with the internal wall permittivity. (a) Relation of  $PL_{obs}$  and  $\gamma$  with the internal wall permittivity. (b) Relation of mean  $\tau_{RMS}$  and mean number of MPCs with the internal wall permittivity.

### 4.3 Different Dielectric Loss Tangent of Internal Wall

The permittivity  $\epsilon_r$  and the thickness  $H$  of the internal wall are fixed to 8 and 12 cm respectively. By changing the dielectric loss tangent  $\tan(\delta)$  of the internal wall, the path loss, RMS delay spread, and number of MPCs change accordingly, and the curves with different  $\tan(\delta)$  of 112 observation points are plotted in Fig. 4, respectively. The  $PL_{obs}$ ,  $\gamma$ , mean  $\tau_{RMS}$  and mean number of MPCs versus  $\tan(\delta)$  are shown in Fig. 5.

From Figs. 4(a) and 5(a), it is clear that the  $PL_{obs}$  increases linearly with the  $\tan(\delta)$  of the internal wall. However, the variation of parameter  $\gamma$  is trivial.

Figs. 4(b) and 5(b) show that the  $\tau_{RMS}$  decreases with the  $\tan(\delta)$  increasing. It means the interference between MPCs becomes smaller when  $\tan(\delta)$  becomes larger. The reason lies in that when the  $\tan(\delta)$  is large enough, some MPCs will disappear.

From Figs. 4(c) and 5(b), it can be seen that the number of MPCs decreases linearly as the  $\tan(\delta)$  increases.

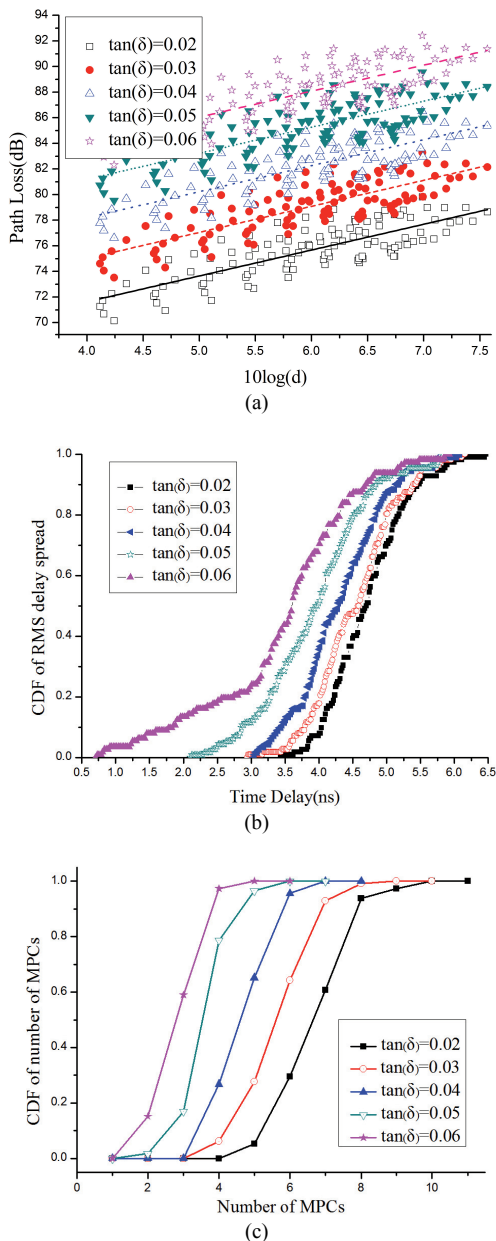


**Fig. 4.** Path-loss model, CDF of RMS delay spread and CDF of number of MPCs for different dielectric loss tangent. (a) Path-loss model for different dielectric loss tangent. (b) CDF of RMS delay spread for different dielectric loss tangent. (c) CDF of number of MPCs for different dielectric loss tangent.

#### 4.4 Different Thickness of Internal Wall

The dielectric constant  $\epsilon_r$  and loss tangent  $\tan(\delta)$  of the internal wall are set to 8 and 0.02 respectively, and the thickness  $H$  changes from 12 cm to 36 cm by a step of 6 cm.

The corresponding path loss, RMS delay spread and number of MPCs of 112 observation points for each thickness are shown in Fig. 6, respectively. Fig. 7 shows

the relation of  $PL_{obs}$ ,  $\gamma$ , mean  $\tau_{RMS}$  and mean number of MPCs with the internal wall thickness  $H$ .

From Figs. 6(a) and 7(a), it can be seen that the  $PL_{obs}$  increases linearly with the increase of  $H$ , and  $\gamma$  is nearly constant for different  $H$ .

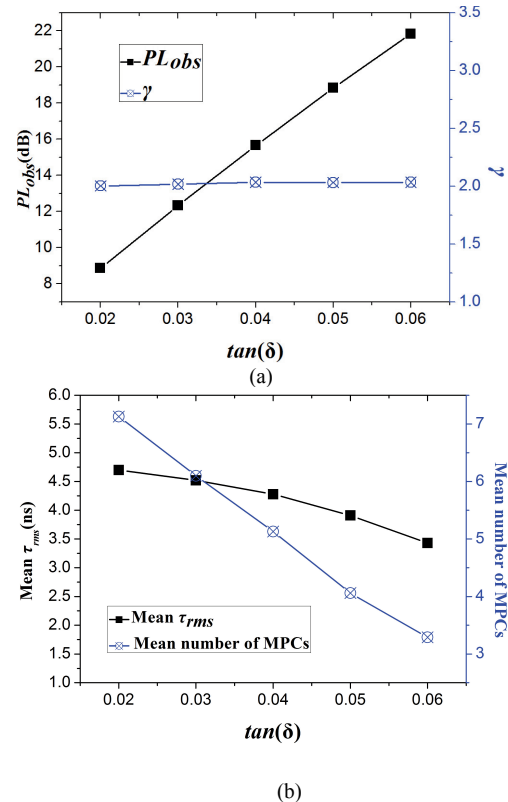


**Fig. 5.** Relation of path loss  $PL_{obs}$ ,  $\gamma$ , mean  $\tau_{RMS}$  and mean number of MPCs, with dielectric loss tangent. (a) Relation of  $PL_{obs}$  and  $\gamma$  with dielectric loss tangent. (b) Relation of mean  $\tau_{RMS}$  and mean number of MPCs, with dielectric loss tangent.

Figs. 6(b) and 7(b) show that when  $H$  increases, the  $\tau_{RMS}$  decreases at first, then increases and reaches a summit when  $H$  is 27 cm; thereafter, when the wall is thicker than 30 cm, the  $\tau_{RMS}$  decreases quickly with the thickening of the wall. In order to demonstrate the phenomenon more explicit, more thickness values have been used to analyze the  $\tau_{RMS}$  variation with different  $H$ , as shown in Fig. 7(b).

The mechanism underlying can be analyzed from the view of the energy carried on each path. When the internal wall is very thin, i.e. thinner than 15 cm, with the thickening of the wall, some MPCs that go through multiple reflections will decay to below the threshold, and then most of the received signal energy is carried by the first path, which results in a smaller  $\tau_{RMS}$ . However, with the further increase of the wall thickness, many MPCs those can arrive at the Rx just go through one reflection and pass through the wall only once, which is true for the first path. Since most energy is carried by the first path, after the signal passes through the wall, most energy decay will occur on the first path. Thus, the received energy is distributed more

even on all MPCs, which results in a larger  $\tau_{RMS}$ . When the wall thickness is larger than 30 cm, if it is thickened furthermore, more MPCs will decay and below the threshold, and then only a few MPCs can be received by the Rx, consequently, the received energy is concentrated on the first path once again, which results in a decrease of  $\tau_{RMS}$ . From the simulation results, it can be seen that in this environment, 15 cm and 27 cm are two turning points of the wall thickness for  $\tau_{RMS}$ .

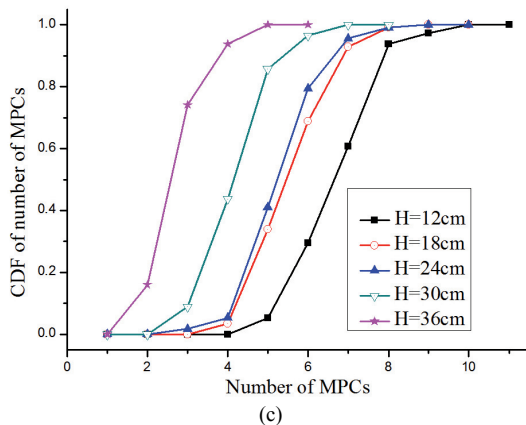
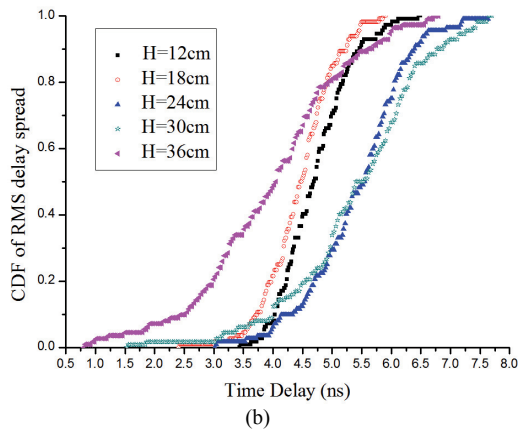
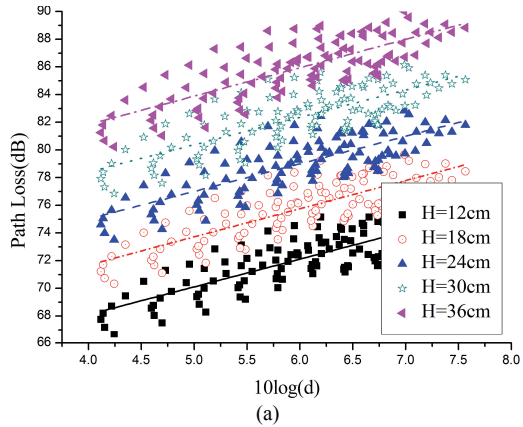


**Fig. 6.** Path-loss model, CDF of RMS delay spread and CDF of number of MPCs for different internal wall thickness. (a) Path-loss model for different internal wall thickness. (b) CDF of RMS delay spread for different internal wall thickness. (c) CDF of number of MPCs for different internal wall thickness.

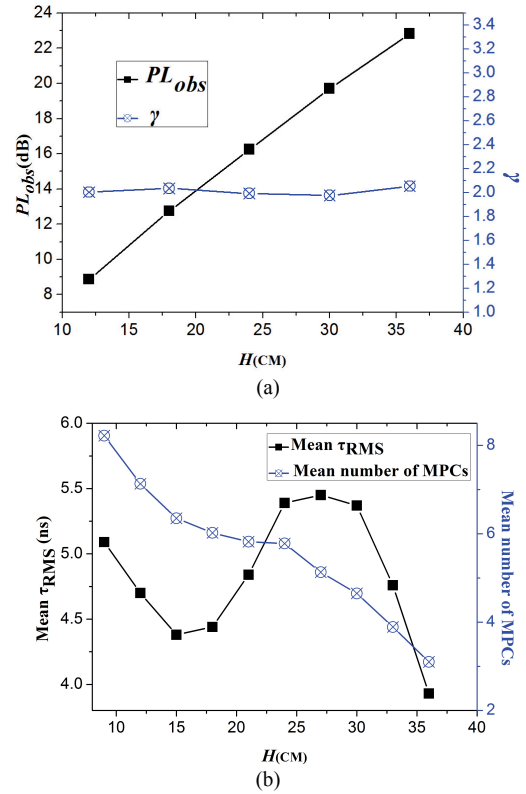


**Fig. 7.** Relation of path loss  $PL_{obs}$ ,  $\gamma$ , mean  $\tau_{RMS}$  and mean number of MPCs, with internal wall thickness. (a) Relation of  $PL_{obs}$  and  $\gamma$  with internal wall thickness. (b) Relation of mean  $\tau_{RMS}$  and mean number of MPCs with internal wall thickness.

From Figs. 6(c) and 7(b), it is shown that the wall thickness has a remarkable effect on the number of MPCs. With the thickening of the internal wall, the signal energy will decay by the wall. Consequently, many MPCs will be below the threshold and treated as the noise, and then the number of MPCs will decrease. When  $H$  increases from 9 cm to 36 cm, the mean number of MPCs linearly decreases from 8.19 to 3.10.

## 5. Comparison between Simulation and Experiment

In order to verify the above mentioned simulation method, a Line of Sight (LOS) channel measurement campaign is carried out in a laboratory located on the 6<sup>th</sup> floor of the Science & Research Building of the University of Electronic Science and Technology of China. As shown in Fig. 8, the J-shaped part is an experimental table with height of 1.2 m. On the table, there are some experimental apparatus and a computer. Both Tx and Rx antennas are planar monopole antennas with omni-directional radiation pattern and at height of 1.5 m. During the measurement, both antennas are kept stationary. The Tx antenna is fixed near the upper right corner, while the Rx antenna is moved at 173 observation points in succession. The whole measurement needs three persons to spend half a day to accomplish.

The same scenario is simulated with the FDTD as well. Based on the measured and simulated data, the path loss decay exponent  $\gamma$  and the mean RMS delay spread are extracted and listed in Tab. 2. It is clear that the data from simulation and measurement agree with each other very well.

In addition, a simulation of electromagnetic wave propagation in vacuum environment has been performed. The computed propagation constant  $\gamma$  is 2.0 in vacuum environment, which is consistent with the theoretical results.

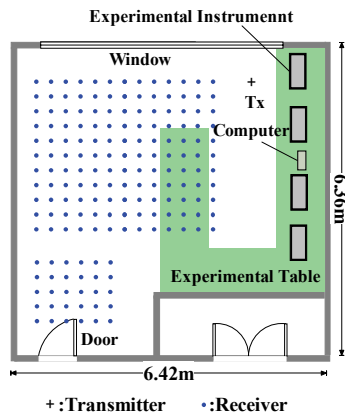


Fig. 8. LOS Scenario for simulation and measurement.

Channel Parameter	$\gamma$	Mean $\tau_{RMS}(ns)$
Measurement	1.73	5.22
Simulation	1.76	4.82

Tab. 2. Measured and simulated channel parameters.

Although only simulation has been performed in the NLOS scenario, both the agreement between the measurement and simulation in the LOS scenario, and the parameters extracted in the vacuum environment, have given a validation of the simulation platform, thus the simulation results in the NLOS scenarios are validated.

## 6. Conclusions

In this paper, the effects of permittivity, dielectric loss tangent and thickness of the internal wall on the indoor wideband wireless channel characteristics have been investigated by using the FDTD method. The results show that the path loss that arise from the obstruction, increases linearly with any of the three internal wall parameters increasing, while the number of MPCs decreases linearly. However, the RMS delay spread is sensitive to the dielectric loss tangent and the thickness of the internal wall, but nothing to do with the wall permittivity. It reduces when the dielectric loss tangent becomes larger, or the internal wall becomes thicker. Through the comparison between the simulation and measurement of the channel characteristics in a LOS environment, and the channel parameters ex-

tracted in a vacuum environment, the simulation investigation has been confirmed.

## Acknowledgements

This work was supported by the Natural Science Foundation of China (61271027, 61331007).

## References

- [1] GHASSEMZADEH, S. S., JANA, R., RICE, C. W., TURIN, W., TAROKH, V. Measurement and modeling of an ultra-wide bandwidth indoor channel. *IEEE Trans. Communications*, Oct. 2004, vol. 52, no. 10, p. 1786-1796.
- [2] TRUEMAN, C. W., DAVIS, D., SEGAL, B., MUNEER, W. Validation of fast site-specific mean-value for indoor propagation. *Applied Computational Electromagnetics Society Journal*, 2009, vol. 24, no. 3, p. 306-317.
- [3] ANNONI, L. A., MINUTOLO, R., MONTANARI, M., SABATINI, T. The Ultra-Wide Bandwidth indoor channel: Measurement campaign and modeling. In *2010 Int. Conference on Software, Telecommunications and Computer Networks*, Sept. 2010, p. 195-199.
- [4] ZHANG, J. H., GAO, X. Y., ZHANG, P., YIN, X. F. Propagation characteristics of wideband MIMO channel in hotspot areas at 5.25 GHz. In *IEEE 18th International Symposium on Personal, Indoor and Mobile Radio Communications*, Sept. 2007, p. 1-5.
- [5] NIE, X., ZHANG, J. H., ZHANG, Y., LIU, G. Y., LIU, Z. M. An experimental investigation of wideband MIMO channel based on indoor hotspot NLOS measurements at 2.35GHz. In *2008 Global Telecommunications Conf.*, Nov. 2008, p. 1-5.
- [6] WANG, S. H., CHEN, X. H., PARINI, C. Ray-tracing based channel model for 5GHz WLAN. In *2009 IEEE Int. Symp. on Antennas and Propagation Society*, June 2009, p. 1-4.
- [7] ZHANG, J. T., HUANG, Y. Indoor channel characteristics comparisons for the same building with different dielectric parameters. In *2002 IEEE Int. Conf. on Communications*, Aug. 2002, p. 916-920.
- [8] XIAO, S. Q., CHEN, J., WANG, B.-Z., LIU, X. A numerical study on time-reversal electromagnetic wave for indoor ultra-wideband signal transmission. In *Progress in Electromagnetics Research, PIER-77*, 2007, p. 329-342.
- [9] ZHAO, Y., HAO, Y., PARINI, C. Two novel FDTD based UWB indoor propagation models. In *2005 IEEE Int. Conf. on Ultra-Wideband*, Sept. 2005, pp. 124-129.
- [10] RAMIREZ, L. A. R., CARVALHO, A. D., TRINTINALIA, L. C., HASSELMANN, F. J. V., MELLO, L. A. R. S. Indoor channel characterization FDTD simulations and measurement. In *2010 Proceedings of the Fourth European Conference on Antennas and Propagation (EuCAP)*, 12-16 April, 2010. p. 1-3.
- [11] LEUNG, J., SARRIS, C. D. On waveguide models of indoor wireless channels insights from FDTD simulations. 2008. *IEEE on Antennas and Propagation Society International Symposium*, 2008. AP-S, 5-11 July, 2008 pp. 1-4.
- [12] WANG, Y., ZHANG, N. T. A New multi-template CLEAN algorithm for UWB channel impulse response characterization. In *2006 Int. Conf. on Communication Technology*, Nov. 2006.

### About Authors ...

**Xue-Song YANG** was born in Hubei province of China. She received the B. Eng. degree from Huazhong University of Science and Technology (HUST), Wuhan, China, and the Ph.D. degree from the UESTC, Chengdu, China. She joined the UESTC in 2002, where she is currently an associate professor. She has been a research fellow at City University of Hong Kong, and a Visiting Scholar at University of Southern California, USA. Her current research interests include reconfigurable antennas, ultra-wideband antennas, and wireless communications channel modeling.

**Zhi-Ming TIAN** received the B. Sc. degree in Physics from Tangshan Normal University, Tangshan, China and the M. Sc degree from UESTC, Chengdu, China. His current research interests include wireless channel modeling and antennas design.

**Jia-Jie YUAN** received the B. E. degree in Polymer Material from Nanchang Hangkong University, Nanchang,

China and the M. Sc. degree in UESTC, Chengdu, China. His current research interests include wireless communications channel modeling.

**Yi-Teng ZHANG** was born in Sichuan province of China. He received his B. Eng. degree from the UESTC, Chengdu, China in 2004. Currently, he is studying for his M. Sc. Degree in the UESTC. His current research interest is wireless channel modeling.

**Wei SHAO** was born in Chengdu, China, in 1975. He received the B. E. degree in Electrical Engineering from UESTC in 1998, and received M. Sc. and Ph. D. degrees in Radio Physics from UESTC in 2004 and 2006, respectively. He joined the UESTC and is now an associate professor there. From 2010 to 2011, he was a Visiting Scholar in the Electromagnetic Communication Laboratory, Pennsylvania State Univ., State College, PA. His research interests include the computational electromagnetic and antenna design.